Computation of current waveform in ferrite power inductors for application in buck-type converters

Carlo Ragusa, Luigi Solimeme, Salvatore Musumeci, Olivier de La Barrière, Fausto Fiorillo, Giulia Di Capua, Nicola Femia

Computation of current waveform in ferrite power inductors for application in buck-type converters

Carlo Ragusa[a], Luigi Solimene[a], Salvatore Musumeci[a], Olivier de la Barriere[b], Fausto Fiorillo[c], Giulia Di Capua[d], Nicola Femia[d]

[a]Department of Energy, Politecnico di Torino, Torino 10129, Italy

[b]Lab. SATIE, CNRS–ENS, 61 avenue du Président Wilson, Cachan, France

[c]Istituto Nazionale di Ricerca Metrologica INRIM, Torino, Italy

[d]Department of Information and Electrical Eng. and Applied Mathematics, University of Salerno, Fisciano (SA), Italy

1. Introduction

Ferrite power inductors find application in DC-DC power converters, because they can store and release energy during the different operating states of the circuit. Present trends in the design of such converters call for higher power densities and smaller volume of the power inductors, because this is usually one of the bulkiest elements in switch-mode power supplies. Following the literature [1], [2], [3], [4], [5], a possible solution consists in the use of inductors working with high values of the magnetic flux density, which would significantly reduce the volume and weight of these components. It has been proved that this solution is viable, if the inductor is not affected by an increase of the magnetic loss density and current ripple exceeding the limits imposed by the application [4]. This happens if the component is selected, or designed, so that its inductance at the maximum rated current of the application is higher than a given minimum value [4]. By this solution, the working conditions of the converter lead the component to operate across a portion of its magnetic characteristic, here represented by flux Φ *versus* current i_L curve, involving a gradual decrease of the flux rate of change $d\Phi/di_L$ for increasing values of the current [6]. Consequently, the current ripple waveform will be influenced by the saturation of the inductor in the circuit model. The accurate analysis of the circuit under such conditions is very important, because amplitude and waveform of the current ripple influence the converter efficiency and control [7]. Such computation is not a trivial task. It requires the measurement of the magnetic characteristic of the inductor up to saturation and the simulation of a nonlinear circuit under a given DC component of the current [8].

Several models and methods have been proposed in recent years, to facilitate the numerical prediction of the inductor operation under large-signal square-wave operating conditions, also involving saturation. In [5], [9], [10], trigonometric functions are adopted to model the differential inductance including saturation, and dedicated iterative numerical methods are proposed to solve the inductor and circuit equations. In [11], the differential inductance is modeled by means of piecewise affine approximations, and the resulting benefits in terms of computational efficiency are discussed. In [12], the current waveform in a DC-DC converter is obtained by application of a commercial circuit simulator.

In this paper, we present a simple and fast numerical method by which the current waveform in a DC-DC buck-type power converter is computed through a successive approximation procedure [13], also known as polarization Fixed Point (FP) method [14], [15]. The results are assessed by comparing experimental waveforms of current and voltage, measured on a commercial DC-DC buck converter, with numerical simulation of the same quantities.

2. Computation of the current waveform in a dc-dc buck converter

A buck converter (or step-down converter) is a DC-DC converter providing an output voltage U_o lower than the input voltage U_i [16], [17], [18]. An example of such circuit is reported in Fig. 1. Here, the single commutation cell consists of a switch (a MOSFET or an IGBT) and a diode. Given the switching period T_s, by controlling the T_{ON} and T_{OFF} time intervals through the duty cycle $d = T_{ON}/T_S$ of the switch in the commutation cell, two different circuital states are cyclically obtained [16], [17].

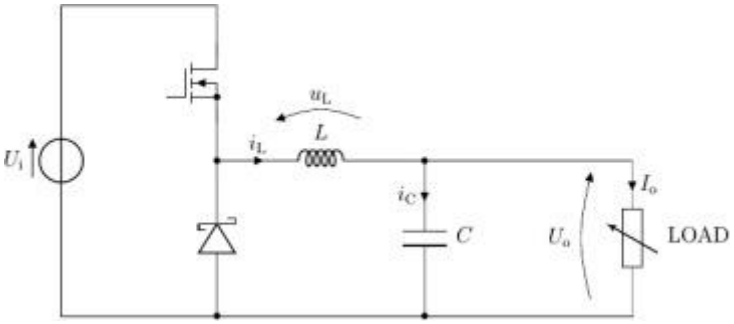

Fig. 1. Schematic of a DC-DC buck converter.

During the ON state, the switch is closed, and the diode is reverse-biased (Fig. 2a); during the OFF state, the switch is open, and the diode is forward-biased (Fig. 2b).

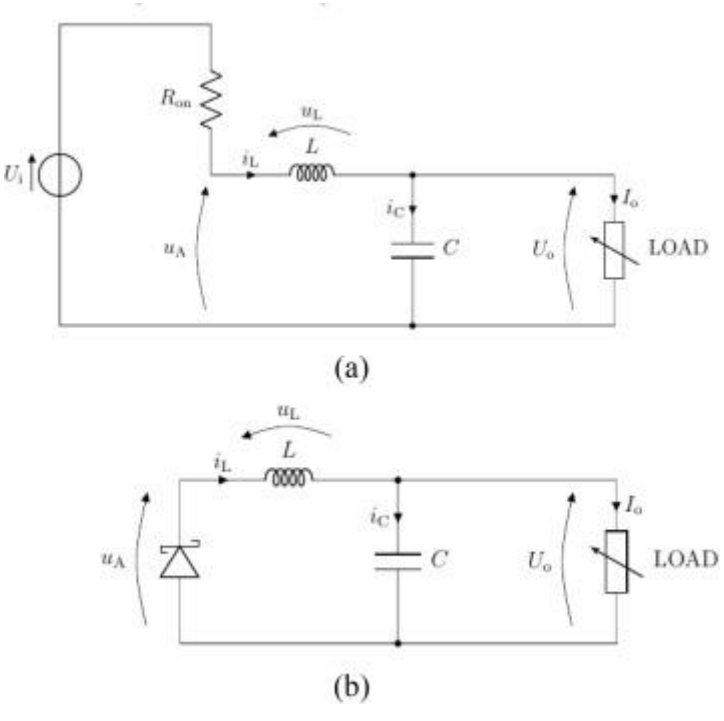

Fig. 2. Equivalent circuit of the buck converter (a) during the ON state and (b) during the OFF state.

During the ON interval ($0 \leq t \leq T_{ON}$, being t the time), the state equation is(1)

where $i_L(t)$ is the current waveform and R_{ON} is the equivalent resistance of the MOSFET during the T_{ON} interval. During the OFF interval ($T_{ON} < t \leq T_S$), the state equation becomes(2)where U_D is the threshold voltage of the diode and R_D is the equivalent differential resistance of the diode. The current $i_L(t)$ is periodic over T_S and the given average current(3)is a constraint of the computation. Because periodic conditions hold, the condition is satisfied, that is(4)

The duty cycle d is obtained from (4) as(5)

In addition, a single valued constitutive equation is assumed as(6)

The periodic current waveform $i_L(t)$ is obtained from the numerical solution of Eqs. (1), (2) under the condition (3), and the constitutive Eq. (6). The solution is achieved through the successive approximation procedure described in the following. First, Eq. (6) is written as(7)

where L_{FP} is a suitable constant and is a residual function. By replacing (7) in (1), (2), we obtain(8)and(9)

Eqs. (8), (9) can now be solved iteratively by application of the FP method [14]. Given the waveform of the residual $i_r^{(k)}$, known from the k-th iteration, Eqs. (8), (9) become(10)

(11)

It is worth noting that

. The analytical solution of (10), (11) can be obtained as(12)(13)where(14)

As

is computed, the current is obtained, according to (7), as(15)and the new residual for the next iteration is eventually obtained as(16)

A suitable numerical computation of the integral terms (12), (13), (14) is applied. At the first iteration step,

is assumed. In addition, the condition(17)always preserves the optimal convergence of the iterative process even in the case of large differences in the differential inductance

[14].

It is worth noting that the described model cannot take into account dissipative effects in the inductor. Such effects could sensibly modify the current waveform. A simple rough correction could be introduced by adding a suitable resistor R_p in parallel to the inductor. Following this approach, the inductor current could be corrected by adding the additional term u_L/R_p. Examples of this correction will be shown in the following section.

3. Results and discussion

The proposed computational method was implemented through the MATLAB® script available in [19]. First, the algorithm was validated by comparing the simulation results of the circuit of Fig. 1, obtained through the proposed algorithm, to simulations obtained through PLECS®, a popular commercial power electronic systems simulator [20]. Such comparisons showed a very good agreement, with discrepancies between the calculated rms currents lower than 0.7 %. The algorithm was then tested by comparing the measured waveforms of the inductor current and voltages - obtained from measurements carried out on a DC-DC buck converter - to numerical simulation of the same quantities, obtained by assuming as input the inductor DC current component. To this end, we tested a commercial DC-DC buck converter, the Texas Instruments TPS54160EVM-230 board [21], with switching frequency f_s = 462.5 kHz, input voltage U_i = 6–60 V, nominal output voltage U_o = 3.3 V and maximum output current I_o = 1.5 A. The original inductor of the board was replaced with a custom inductor, made of a toroidal core of N30 ferrite (manufacturer TDK [22]), of size 20 × 10 × 7 mm^3, endowed with five turns, whose magnetic properties were measured in advance [23]. The relevant curves, providing the flux versus magnetizing current and the differential inductance profile, are shown in Fig. 3. The scheme of the experimental setup is given in Fig. 4. Here, the duty cycle is set to automatically regulate the output voltage U_o to ≈3.3 V, the output current I_o can be regulated up to 1.5 A through the electronic load (Rigol DL3031), and the voltage U_i can be changed between 6 and 60 V. The eight test cases described in Table 1 were adopted to cover regimes extending up to the saturation of the inductor under test. The current was measured through a current probe, and the voltage across the inductor was obtained by difference between the voltages U_A and U_o. The average power loss P_L dissipated in the inductor, obtained as the difference between the injected power P_A and the output power P_o, is reported in Table 1.

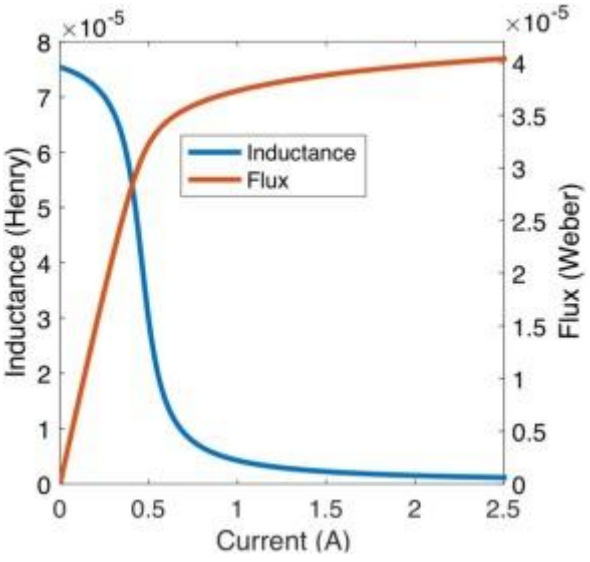

Fig. 3. Differential inductance and flux vs. current in the ferrite toroidal core inductor TDK - N30 [22] of size 20 × 10 × 7 mm^3 with five-turn windings.

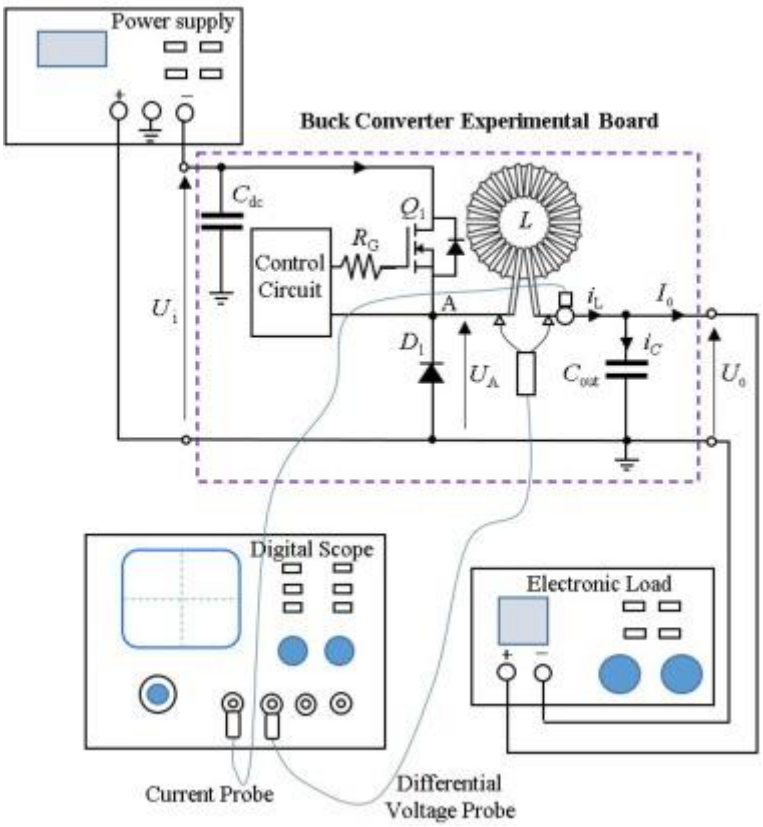

Fig. 4. Scheme of the applied experimental setup containing the commercial buck converter board [21] and the custom ferrite core toroidal inductor (TDK – N30) [22]. The output current I_o can be regulated up to 1.5 A through the electronic load Rigol DL3031, and the voltage U_i can be changed between 6 V and 60 V. The output voltage is automatically regulated at U_o = 3.3 V through the duty cycle.

Table 1. Operating conditions for the DC-DC buck converter TPS54160EVM-230 board.

Test case	U_i **(V)**	U_o **(V)**	I_o **(A)**	f_s **(kHz)**	P_L **(mW)**	R_p **(Ω)**
#1	15	3.325	0.209	462.5	76.5	589
#2	15	3.325	0.300	462.5	82.9	548
#3	15	3.324	0.411	462.5	87.5	521
#4	15	3.326	0.714	462.5	102.7	446
#5	25	3.288	0.195	462.5	144.5	588
#6	25	3.273	0.390	462.5	149.5	577
#7	25	3.273	0.491	462.5	154.4	563
#8	25	3.264	0.589	462.5	156.1	558

The equivalent parallel resistance R_p, by which dissipative effect could be simulated, was computed as(18)

The current and voltage waveforms were simulated adopting the parameters of Table 1. In addition, it is R_{ON} = 0.3 Ω, R_D = 0.05 Ω, and U_D = 0.5 V. Fig. 5, Fig. 6 show several comparisons of experimental measurements of the inductor voltage and current, and the relevant theoretical results obtained by means of the proposed approach, in the eight case

studies listed in Table 1. About 30 iteration steps are needed to reach convergence. The computed current was corrected *a posteriori*, by adding the term u_L/R_p. By this term, the jump of the current at switching is taken into account.

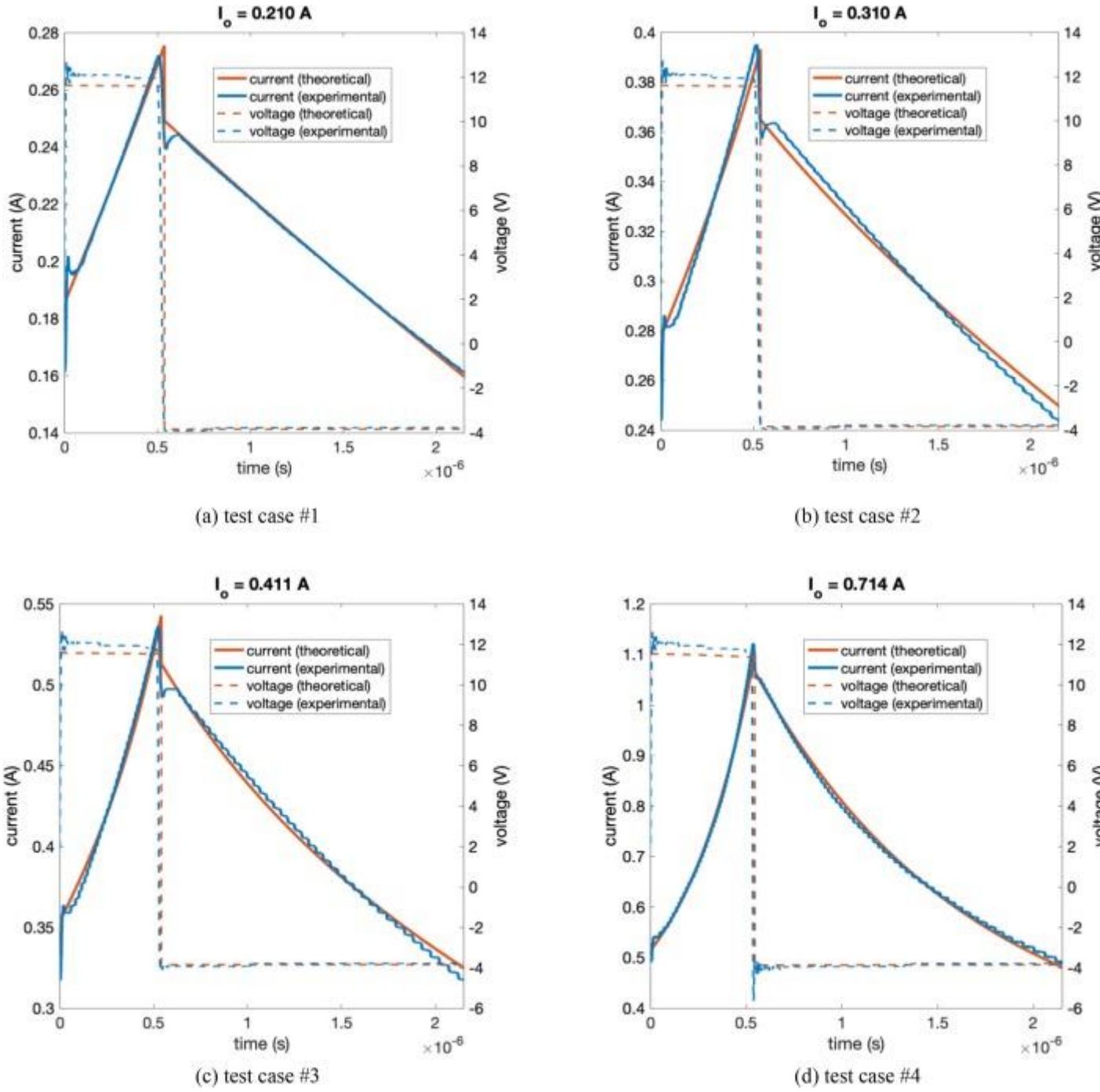

(a) test case #1 (b) test case #2

(c) test case #3 (d) test case #4

Fig. 5. Comparison between experimental and theoretical waveforms of the current i_L and voltage u_L in the tested DC-DC buck converter [21] adopting the custom ferrite inductor [22]. About 30 iteration steps are needed to reach convergence. The results refer to the case of test from #1 to #4 of Table 1 with U_i = 15 V. Here, I_o is the average current in the inductor. The computed current was corrected *a posteriori* by adding the term u_L/R_p. By this term, the jump of the current at switching is taken into account.

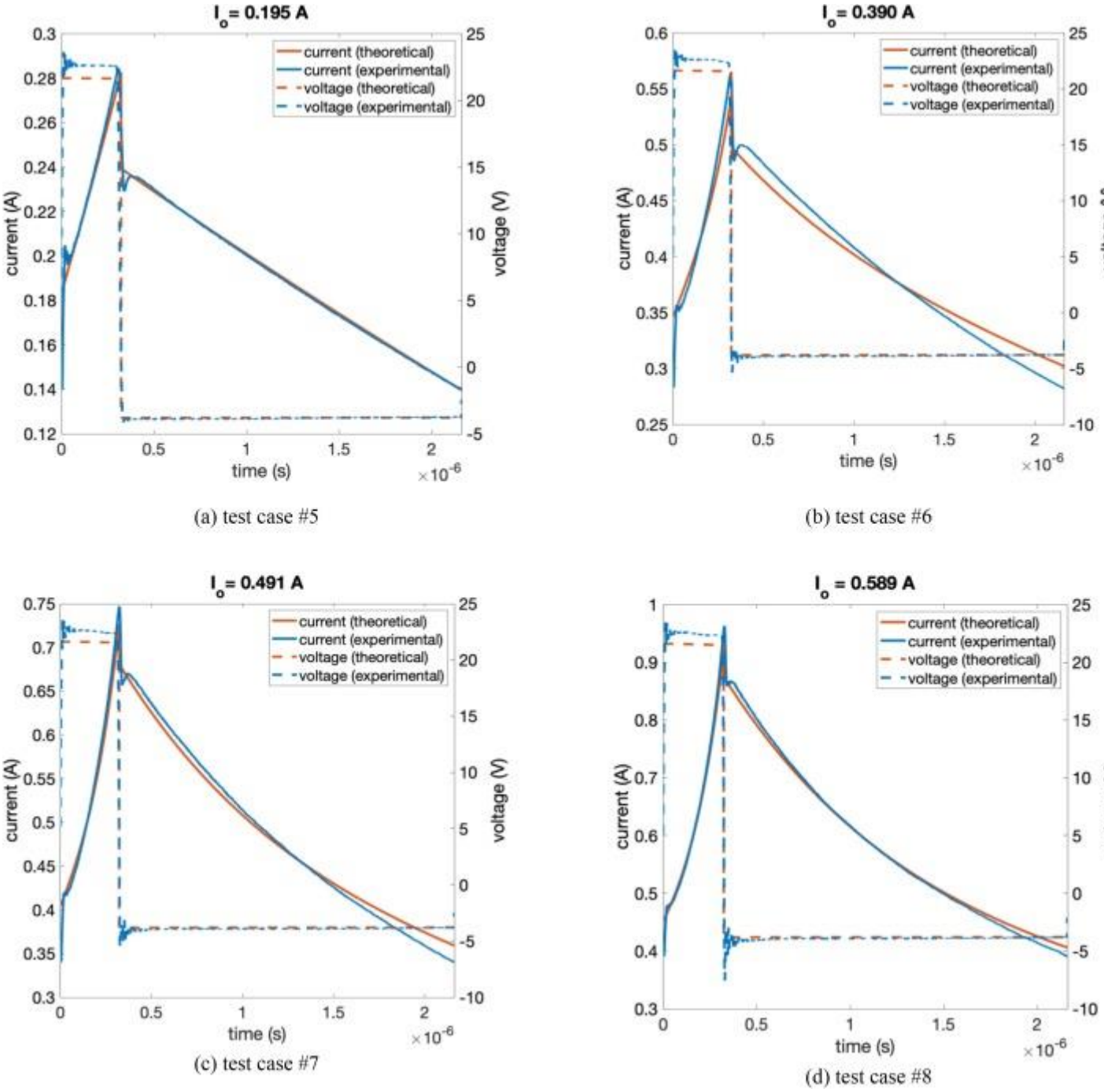

Fig. 6. Comparison between experimental and theoretical waveforms of the current i_L and voltage u_L in the tested DC-DC buck converter [21] adopting the custom ferrite inductor [22], as in Fig. 5. The results refer to the case of test from #5 to #8 of Table 1 with U_i = 25 V.

The experimental results validate the computational method for the analysis of ferrite power inductors in buck-type converters with the proposed numerical approach easily extendable to other DC-DC topologies. Thanks to the current waveform approximation, it could be possible to correctly predict the peak-to-peak ripple current, also under partial saturation operating conditions.

4. Conclusions

In this paper we presented a simple and fast numerical method by which the current waveform in a DC-DC buck-type power converter is computed through a successive approximation procedure, taking into account the nonlinear magnetic characteristic of the inductor. The proposed algorithm has been preliminarily validated through a comparison to the commercial simulator PLECS®. The obtained theoretical results have been compared to measurements made on a commercial DC-DC buck converter, where the original inductor of the board was replaced with a custom inductor. The proposed method is simple, fast, and the convergence is always preserved despite the strong non-linearity of the inductor.

References

[1]
H. Wang, M. Liserre, F. Blaabjerg**Toward Reliable Power Electronics: Challenges, Design Tools, and Opportunities**
IEEE Ind. Electron. Mag., 7 (2) (2013), pp. 17-26, 10.1109/MIE.2013.2252958

[2]
F. Bizzarri, A. Brambilla, L. Codecasa, S. Callegari**On the Benefit of Adopting Saturable Inductors in Switching-Mode Power-Supplies: A Case Study**
2018 IEEE International Symposium on Circuits and Systems (ISCAS), IEEE (2018), pp. 1-5, 10.1109/ISCAS.2018.8351574

[3]
L. Milner, G.A. Rincón-Mora**Small saturating inductors for more compact switching Power Supplies**
IEEJ Trans. Electr. Electron. Eng., 7 (1) (2012), pp. 69-73, 10.1002/tee.21697

[4]
G. Di Capua, N. Femia, K. Stoyka**Switching Power Supplies with Ferrite Inductors in Sustainable Saturation Operation**
Int. J. Electr. Power Energy Syst., 93 (2017), pp. 494-505,
10.1016/j.ijepes.2017.06.003
Article

[5]
G. Di Capua, N. Femia**A Novel Method to Predict the Real Operation of Ferrite Inductors with Moderate Saturation in Switching Power Supply Applications**
IEEE Trans. Power Electron., 31 (3) (2016), pp. 2456-2464,
10.1109/TPEL.2015.2438952

[6]
K. Detka, K. Gorecki, J. Zarebski**Modeling single inductor DC-DC converters with thermal phenomena in the inductor taken into account**
IEEE Trans. Power Electron., 32 (9) (2017), pp. 7025-7033,
10.1109/TPEL.2016.2628202

[7]
K. Górecki, K. Detka**Application of average electrothermal models in the SPICE-aided analysis of boost converters**
IEEE Trans. Ind. Electron., 66 (4) (2019), pp. 2746-2755, 10.1109/TIE.2018.2847694
CrossRefView Record in ScopusGoogle Scholar

[8]
J.D. Pollock, W. Lundquist, C.R. Sullivan**Predicting inductance rolloff with dc excitations**
IEEE Energy Convers. Congress Exposition (ECCE) (2011), pp. 2139-2145,
10.1109/ECCE.2011.6064051

[9]
A. Oliveri, G. Di Capua, K. Stoyka, M. Lodi, M. Storace, N. Femia**"A Power-Loss-Dependent Inductance Model for Ferrite-Core Power Inductors in Switch-Mode Power Supplies**
IEEE Trans. Circuits Syst. I: Reg. Papers, 66 (6) (2019), pp. 2394-2402, 10.1109/TCSI.2018.2889856

[10]
F. Bizzarri, A. Brambilla, A.E. Aroudi**Nonlinear Analysis of a DC-DC Boost Converter Working as a Maximum Power Point Tracker using Analog-Mixed-Signal Circuit Simulation**
2019 IEEE Int. Symposium on Circuits and Systems (ISCAS), IEEE, Sapporo, Japan (2019), pp. 1-5, 10.1109/ISCAS.2019.8702182

[11]
A. Oliveri, M. Lodi, M. Storace**A Piecewise-Affine Inductance Model for Inductors Working in Nonlinear Region**
2019 16th International Conference on Synthesis, Modeling, Analysis and Simulation Methods and Applications to Circuit Design (SMACD), IEEE (2019), pp. 169-172 Lausanne, Switzerland, July 2019. DOI: 10.1109/SMACD.2019.8795270

[12]
R.A. Salas, J. Pleite, E. Olías, A. Barrado**Theoretical–experimental comparison of a modeling procedure for magnetic components using finite element analysis and a circuit simulator**
J. Mag. Mag. Mater., 320 (20) (2008), pp. e1024-e1028, 10.1016/j.jmmm.2008.04.124 Article

[13]
F. Hantila, Electromagnetic Field in Non-Linear Media, [online]. Available: http://www.mathem.pub.ro/bjga/v04n2/B04-2-HANTILA2.pdf.

[14]
F.I. Hantila, G. Preda, M. Vasiliu**Polarization method for static fields**
IEEE Trans. Mag., 36 (4) (2000), pp. 672-675, 10.1109/20.877538

[15]
I.R. Ciric, F.I. Hantila**An Efficient Harmonic Method for Solving Nonlinear Time-Periodic Eddy-Current Problems**
IEEE Trans. Mag., 43 (4) (2007), pp. 1185-1188, 10.1109/TMAG.2006.890952

[16]
R. Erickson, D. Maksimović, Fundamentals of Power Electronics, KAP, 2nd ed., 2001.

[17]
P. Wilson, H. Alan Mantooth, Chapter 9 – Fast Analog Modeling, Model-Based Engineering for Complex Electronic Systems, pp. 305–346, Newnes, 2013, ISBN 9780123850850. https://doi.org/10.1016/B978-0-12-385085-0.00009-9.

[18]
R. Bojoi, F. Fusillo, A. Raciti, S. Musumeci, F. Scrimizzi, S. Rizzo**Full-Bridge DC-DC Power Converter for Telecom applications with Advanced Trench Gate MOSFETs**
2018 IEEE Int. Telecom-Munications Energy Conf. (INTELEC), IEEE, Turin (2018), pp. 1-7, 10.1109/INTLEC.2018.8612309

[19]

C. Ragusa, L. Solimene, MATLAB® script for the computation of current waveform in ferrite power inductors for application in buck-type converters, [online]. Available: https://github.com/Luigi-Solimene/Inductor-current-computation-in-buck-converter.

[20] PLECS®, The Simulation Platform for Power Electronic Systems [online]. Available: https://www.plexim.com/plecs.

[21] TPS54160EVM-230 evaluation module (EVM) [online]. Available: http://www.ti.com/tool/TPS54160EVM-230.

[22] SIFERRITE Material N30 [online]. Available: https://www.tdk-electronics.tdk.com/download/187204/11a3ca92549b8d3b7cce210eace3dc3c/pdf-n30.pdf.

[23] C. Ragusa, L. Solimene, S. Musumeci, O. de la Barrière, F. Fiorillo**Modeling of Saturable Inductors for Application in DC-DC Converters**
2019 26th IEEE International Conference on Electronics, Circuits and Systems (ICECS), IEEE, Genoa, Italy (2019), pp. 839-842, 10.1109/ICECS46596.2019.8964948